Journal of Computational and Applied Mathematics 235 (2011) 4174–4186

Contents lists available at ScienceDirect

Journal of Computational and Applied Mathematics

journal homepage: www.elsevier.com/locate/cam

A general algorithm for the numerical evaluation of nearly singular integrals on 3D boundary element

Xianyun Qin, Jianming Zhang *, Guizhong Xie, Fenglin Zhou, Guanyao Li

State Key Laboratory of Advanced Design and Manufacturing for Vehicle Body, College of Mechanical and Vehicle Engineering, Hunan University, Changsha 410082, China

ARTICLE INFO

Article history:
Received 30 September 2010
Received in revised form 27 December 2010

Keywords:
Nearly singular integrals
Numerical integration
Boundary integral equations
Distance transformation technique

ABSTRACT

A general numerical method is proposed to compute nearly singular integrals arising in the boundary integral equations (BIEs). The method provides a new implementation of the conventional distance transformation technique to make the result stable and accurate no matter where the projection point is located. The distance functions are redefined in two local coordinate systems. A new system denoted as (α, β) is introduced here firstly. Its implementation is simpler than that of the polar system and it also performs efficiently. Then a new distance transformation is developed to remove or weaken the near singularities. To perform integration on irregular elements, an adaptive integration scheme is applied. Numerical examples are presented for both planar and curved surface elements. The results demonstrate that our method can provide accurate results even when the source point is very close to the integration element, and can keep reasonable accuracy on very irregular elements. Furthermore, the accuracy of our method is much less sensitive to the position of the projection point than the conventional method.

1. Introduction

Accurate evaluation of boundary integrals with various kernel functions of the type $O(1/r^{\chi})$ is an important issue in the implementation of the boundary type numerical methods based on the boundary integral equations (BIEs), such as the boundary element method (BEM), the boundary face method (BFM) [1]. r is the distance between the source point and the field point. These integrals become singular or nearly singular when the source point collides with or is close to the field point. The conventional Gaussian quadrature becomes inefficient or even inaccurate to evaluate these integrals. Special integration techniques are urgently needed to deal with these integrals. In this work, we focus on numerical evaluation of nearly singular integrals in three dimensions.

The nearly singular integral arises in mainly five cases: (a) the concerned structure is thin [2,3]; (b) the neighboring element sizes of a surface are quite different [4]; (c) the element's shape is very irregular [1]; (d) the interior points are close to the boundary in the post-processing; (e) for crack problems. In most cases the number of the nearly singular integrals can be much larger than that of the singular integrals in computation of the system matrix, because the singular integrals are involved in the evaluation of the main diagonal entries only. Therefore, efficient and accurate evaluation of the nearly singular boundary integrals may be a key factor in the overall performance of the BEM or BFM [5].

To remove the near singularities, various methods have been proposed, such as the element subdivision technique [1,6], analytical and semi-analytical methods [7,8], non-linear transformation techniques [9–16] and distance transformation techniques [17–19]. The element subdivision method is accurate but inefficient, and may be instable when the distance

* Corresponding address: College of Mechanical and Vehicle Engineering, Hunan University, Changsha 410082, China. Tel.: +86 731 88823061.
E-mail address: zhangjianm@gmail.com (J. Zhang).

0377-0427/$ – see front matter © 2011 Elsevier B.V. All rights reserved.
doi:10.1016/j.cam.2011.03.012

is very small compared with the element size. The analytical and semi-analytical methods are effective, but are limited to the planar elements only. When curved elements are involved, these elements must be divided into a large number of planar triangles, thus losing efficiency and accuracy. Most variable transformation techniques are efficient. However, it is difficult to find a general method which is effective for a wide range of nearly singular integrals and can be used to compute nearly singular integrals on different boundary elements. Moreover, these methods are dependent on kernel functions, and complicated mathematical deductions for different kernels are required. Distance transformation method [17,18], which has been proposed by Ma et al., is a general strategy to deal with nearly singular integrals with various kernels in BEM. This promising method is derived from Guiggiani's excellent work for dealing with singular boundary integrals [19]. For this method, the numerical results are very sensitive to the position of the projection point of the source point. This is also the common drawback of the methods discussed above. Moreover, the projection point is defined in a rigorous way, namely, the line consisting of the source point and the projection point must be perpendicular to the tangential plane through the projection point for 3D boundary elements. According to the definition, the following two difficult cases may be encountered. If the source point is located inside the tangential plane through the projection point [17], the method fails when the transformation is performed based on the local Cartesian coordinate system. If the projection point is located outside the element, troubles may be introduced due to the complexity of determining the local variable ρ and θ intervals of the local poplar system. It is necessary to consider both the position of the projection point (e.g. outside or inside the element) and the element's shape (e.g. triangle or quadrangle).

In this paper, we present a new implementation of the distance transformation technique, and extend the technique to evaluate nearly singular integrals on parametric surface elements used in BFM [1,20]. In our implementation, the projection point of the source point is defined in a more general form. The troubles detailed above are circumvented using our method. What is more, our method has an attractive feature that its accuracy is much less sensitive to the position of the projection point. This performance makes our method is very practical in actual problems. We also introduce a new local coordinate system [1,20] described by (α, β) into the area of nearly singular integration firstly. This system is similar to the polar system, but its implementation is simpler than the polar system and it also performs efficiently. To deal with nearly singular integrals on slender surface elements, the element subdivision technique is employed here in combination with our method. Although element subdivision is adopted, the computational cost is reduced dramatically compared with the conventional subdivision techniques [1,6,20].

The goal of our work is to develop a general method that is suitable for various 3D boundary elements including planar and curved surface elements and very irregular elements with slender shape in physical space. In this paper, we deal with integrals with near weak and strong singularities appearing in BIEs, and the evaluation of nearly hypersingular integrals will be reported in a forthcoming paper.

2. Statement of the problem

In this paper, we deal with the following boundary integral with near singularity over 3D boundary element S:

$$I = \int_S \frac{f(\mathbf{y}, r)}{r^{\chi}} \phi(\mathbf{x}) \mathrm{d}S(\mathbf{x}), \quad \chi = 1, 2 \tag{1}$$

where $\mathbf{y}$ and $\mathbf{x}$ are referred to as the source point and the field point in BEM or BFM, respectively, $\mathbf{y}$ is very close to S, r is the Euclidean distance between $\mathbf{y}$ and $\mathbf{x}$, f is a well-behaved function, and $\phi(\mathbf{x})$ is a shape function. Since $\mathbf{y}$ is outside the integration element S but very close to it, the integrals (1) become nearly singular. This problem usually is referred to as the boundary layer effect in BEM.

Now, we consider the boundary integral equations of 3D potential problems in the domain Ω enclosed by the boundary Γ. The two basic functions are presented in terms of the flux q and potential u on the boundary as follows [17]:

$$c(\mathbf{y})u(\mathbf{y}) = \int_\Gamma q(\mathbf{x})u^*(\mathbf{x}, \mathbf{y})\mathrm{d}\Gamma(\mathbf{x}) - \int_\Gamma u(\mathbf{x})q^*(\mathbf{x}, \mathbf{y})\mathrm{d}\Gamma(\mathbf{x}) \tag{2}$$

$$c(\mathbf{y})u_k(\mathbf{y}) = \int_\Gamma q(\mathbf{x})u_k^*(\mathbf{x}, \mathbf{y})\mathrm{d}\Gamma(\mathbf{x}) - \int_\Gamma u(\mathbf{x})q_k^*(\mathbf{x}, \mathbf{y})\mathrm{d}\Gamma(\mathbf{x}) \tag{3}$$

where c is a coefficient depending on the smoothness of the boundary at the source point $\mathbf{y}$. $u^*(\mathbf{x}, \mathbf{y})$ is the fundamental solution for the 3D problem expressed as

$$u^*(\mathbf{x}, \mathbf{y}) = \frac{1}{4\pi}\frac{1}{r(\mathbf{x}, \mathbf{y})}. \tag{4}$$

And $q^*(\mathbf{x}, \mathbf{y})$, $u_k(\mathbf{x}, \mathbf{y})$ and $q_k^*(\mathbf{x}, \mathbf{y})$ are all the derived fundamental solutions

$$q^*(\mathbf{x}, \mathbf{y}) = \frac{\partial u^*(\mathbf{x}, \mathbf{y})}{\partial \mathbf{n}}, \qquad u_k^*(\mathbf{x}, \mathbf{y}) = \frac{\partial u^*(\mathbf{x}, \mathbf{y})}{\partial x_k} \qquad q_k^*(\mathbf{x}, \mathbf{y}) = \frac{\partial q^*(\mathbf{x}, \mathbf{y})}{\partial x_k} \tag{5}$$

where $\mathbf{n}$ is the unit outward normal direction to the boundary Γ, with components n_i, $i = 1, 2, 3$.

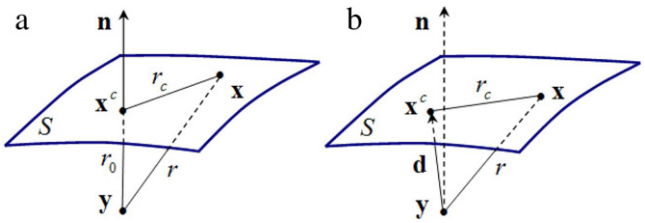

Fig. 1. Definitions of the projection point $\mathbf{x}^c$ of the source point $\mathbf{y}$: (a) conventional definition; (b) improved definition.

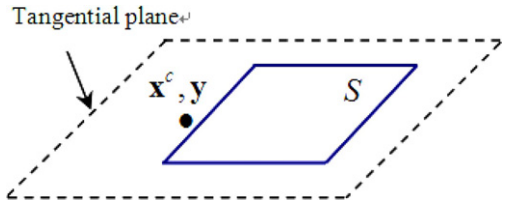

Fig. 2. A case for $r_0 = 0$, the conventional transformation fails.

To numerically evaluate boundary integrals for Eqs. (2) and (3), the boundary Γ is divided into a number of surface elements. Then boundary integration is performed on each element as Eq. (1). Nearly singular integrals arise whenever the source point is close to the integration element. Eqs. (2) and (3) become near singularities with different levels, namely, u^* with near weak singularity, u_k^* and q^* with near strong singularity, and q_k^* with near hyper-singularity.

In this paper, we develop a new implementation of the distance transformation technique. The implementation is detailed in the following sections. For the sake of clarity and brevity for discussion, the following integral in general form is used here.

$$I = \int_S O(1/r^{\chi})\phi \mathrm{d}S. \tag{6}$$

3. Construct new distance functions

3.1. Define the projection point in a general form

In this section, we make a novel definition for the projection point of the source point taking an inspiration from the works of Ref. [17,18]. This is an important point for introducing our new ideas for constructing distance functions in the next subsection.

Fig. 1(a) illustrates the definition of the projection point $\mathbf{x}^c$ of the source point $\mathbf{y}$ in Ref. [17]. This definition is more rigorous. It is clearly found that the line with end points $\mathbf{x}^c$ and $\mathbf{y}$ is perpendicular to the tangential plane through $\mathbf{x}^c$ (not shown in Fig. 1(a)). As shown in Fig. 1(b), a novel definition of the projection point is described in a general form. A new vector $\mathbf{d}$ (with components d_k, $k = 1, 2, 3$) form $\mathbf{y}$ to $\mathbf{x}^c$ is constructed additionally, which is not required to be perpendicular to the tangential plane through $\mathbf{x}^c$ (not shown in Fig. 1(b)).

Applying the first-order Taylor expansion in the neighborhood of $\mathbf{x}^c$ for the conventional definition in Ref. [17], we have

$$x_k - y_k = x_k - x_k^c + x_k^c - y_k = \frac{\partial x_k}{\partial t_1}\bigg|_{\substack{t_1=c_1\\ t_2=c_2}} (t_1 - c_1) + \frac{\partial x_k}{\partial t_2}\bigg|_{\substack{t_1=c_1\\ t_2=c_2}} (t_2 - c_2) + r_0 n_k(c_1, c_2) + O(\rho^2) \tag{7}$$

where c_1, c_2 are the coordinates of the projection point in a local system (t_1, t_2), $\rho = \sqrt{(c_1 - t_1)^2 + (c_2 - t_2)^2}$, and $r_0 = \|\mathbf{x}^c - \mathbf{y}\|$ which is the minimum distance from the source point to the element in most cases. r_0 equals zero whenever $\mathbf{y}$ is located inside the tangential plane through $\mathbf{x}^c$ (see Fig. 2). For this case, the transformation from Ref. [17] in (t_1, t_2) system fails (actually described by (ξ_1, ξ_2) in Ref. [17]). This problem will arise in the following three cases in BEM model (seen Fig. 3): (a) the element distribution is irregular; (b) discontinuous elements are employed; (c) the neighboring element sizes of a surface are quite different.

Again, applying the first-order Taylor expansion in the neighborhood of $\mathbf{x}^c$ for our novel strategy, we have

$$x_k - y_k = x_k - x_k^c + x_k^c - y_k = \frac{\partial x_k}{\partial t_1}\bigg|_{\substack{t_1=c_1\\ t_2=c_2}} (t_1 - c_1) + \frac{\partial x_k}{\partial t_2}\bigg|_{\substack{t_1=c_1\\ t_2=c_2}} (t_2 - c_2) + d_k + O(\rho^2). \tag{8}$$

The following notes are made for the improved definition when compared with the conventional method in Ref. [17]:

- The projection point is just located inside the integration element or on an element's edge or vertex. The distance $\|\mathbf{d}\| = \|\mathbf{x}^c - \mathbf{y}\|$ is the minimum distance from the source point to the element, which is positive.

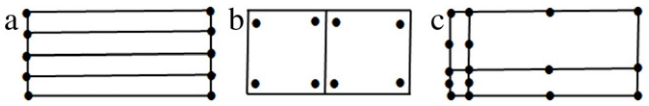

Fig. 3. Three types of the element patterns introducing nearly singular integrals: (a) Irregular element distribution; (b) Discontinuous elements; (c) Element sizes are quite different.

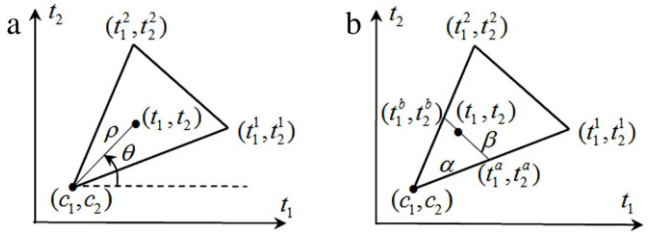

Fig. 4. Two local coordinate systems in (t_1, t_2) parametric space used to define distance functions: (a) polar system (ρ, θ); (b) new system (α, β).

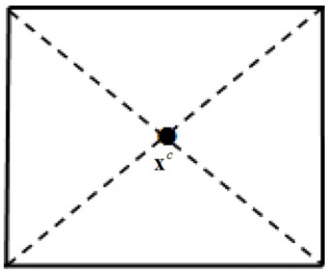

Fig. 5. Subdivisions of a quadrilateral element when $\mathbf{x}^c$ is located at its center.

- In case $\|\mathbf{d}\|$ is the minimum distance, $\mathbf{x}^c$ coincides with the 'ideal projection point'. This is a prerequisite condition in the conventional method. However, $\mathbf{x}^c$ in formulation (8) is an arbitrary point. Using formulation (8) can get accurate results even if $\mathbf{x}^c$ is a little far away from the 'ideal projection point'. This property is particularly beneficial when solving real-world problems in which the ideal location of $\mathbf{x}^c$ usually cannot be accurately calculated.
- Since the minimum distance is not equal to zero ($r_0^2 = \|\mathbf{d}\|$), the transformation given by Ref. [17] in (ξ_1, ξ_2) system is always valid using our modified definition.
- No projection point is located outside the integration element, which makes it convenient to determine integration variables' limits in the local polar system (ρ, θ).

3.2. Construct distance functions

Based on the improved definition of the projection point and the Taylor expansion (8) in the previous subsection, distance functions can be easily constructed. In this section, we introduce two local coordinate systems, namely the polar system (ρ, θ) and a new system (α, β) as shown in Fig. 4, for constructing two different distance functions. The local system (α, β) was first proposed by Zhang et al., to deal with weakly singular integrals in Ref. [1], which is employed here to construct distance functions.

Before constructing distance functions, we first split the integration element into several triangles considering the position of projection point $\mathbf{x}^c$. Each triangle is with $\mathbf{x}^c$ as one of its vertices. Taking an example, as shown in Fig. 5, a quadrilateral element is split into four triangles when $\mathbf{x}^c$ is located at its center. The details on how to split an element in a suitable pattern considering arbitrary position of $\mathbf{x}^c$ will be discussed in Section 4.2. Then distance functions are built in each triangle.

In the (ρ, θ) system as shown in Fig. 4(a), t_1 and t_2 can be expressed as

$$\begin{cases} t_1 = c_1 + \rho\cos\theta \\ t_2 = c_2 + \rho\cos\theta \end{cases} \tag{9}$$

where c_1 and c_2 are local coordinates of the projection point $\mathbf{x}^c$ in the (t_1, t_2) system.

Substituting Eq. (9) into Eq. (8) yields

$$x_k - y_k = x_k - x_k^c + x_k^c - y_k = \rho A_k(\theta) + d_k + O(\rho^2) \tag{10}$$

where

$$A_k(\theta) = \left.\frac{\partial x_k}{\partial t_1}\right|_{\substack{t_1=c_1\\ t_2=c_2}} \cos\theta + \left.\frac{\partial x_k}{\partial t_2}\right|_{\substack{t_1=c_1\\ t_2=c_2}} \sin\theta. \tag{11}$$

Using Eq. (10), the real distance between the source point and the field points can be written as

$$r^2 = A_k^2(\theta)\rho^2 + 2d_kA_k(\theta)\rho + |\mathbf{d}|^2 + O(\rho^3) = a\left[\left(\rho + \frac{b}{2a}\right)^2 + \frac{r_0^2}{a} - \left(\frac{b}{2a}\right)^2\right] + O(\rho^3) \tag{12}$$

where

$$a = A_k^2(\theta) > 0, \qquad b = 2d_kA_k(\theta), \qquad r_0^2 = |\mathbf{d}|^2. \tag{13}$$

Similarly to Ref. [17], the following distance function can be given as

$$g(\rho,\theta) = \sqrt{\left(\rho + \frac{b}{2a}\right)^2 + \delta^2} \tag{14}$$

where

$$\delta^2 = \frac{r_0^2}{a} - \left(\frac{b}{2a}\right)^2 > 0. \tag{15}$$

To construct the local (α, β) system as shown in Fig. 4(b), the following mapping is used:

$$\begin{cases} t_1^a = t_1^0 + (t_1^1 - c_1)\alpha \\ t_2^a = t_2^0 + (t_2^1 - c_2)\alpha \end{cases} \tag{16a}$$

$$\begin{cases} t_1^b = t_1^0 + (t_1^2 - c_1)\alpha \\ t_2^b = t_2^0 + (t_2^2 - c_2)\alpha \end{cases} \tag{16b}$$

$$\begin{cases} t_1 = t_1^a + (t_1^b - t_1^a)\beta \\ t_2 = t_2^a + (t_2^b - t_2^a)\beta \end{cases} \quad \alpha, \beta \in [0, 1]. \tag{16c}$$

Combining Eqs. (16a)–(16c), the expression for obtaining coordinates t_1 and t_2, which is different from that of the polar system, can be written as

$$\begin{cases} t_1 = c_1 + (t_1^1 - c_1)\alpha + (t_1^2 - t_1^1)\alpha\beta \\ t_2 = c_2 + (t_2^1 - c_2)\alpha + (t_2^2 - t_2^1)\alpha\beta. \end{cases} \tag{17}$$

The Jacobian of the transformation from the (t_1, t_2) system to the (α, β) system is αS_Δ, and

$$S_\Delta = \left|t_1^1t_2^2 + t_1^2c_2 + c_1t_2^1 - t_1^2t_2^1 - c_1t_2^2 - t_1^1c_2\right| \tag{18}$$

which keeps constant over the triangle.

In a similar manner, the real distance between the source point and the field points in (ρ, θ) system, can be expressed as

$$\begin{aligned} r^2 &= A_k^2(\beta)\alpha^2 + 2d_kA_k(\beta)\alpha + |\mathbf{d}|^2 + O(\alpha^3) \\ &= a\left[\left(\alpha + \frac{b}{2a}\right)^2 + \frac{r_0^2}{a} - \left(\frac{b}{2a}\right)^2\right] + O(\alpha^3) \end{aligned} \tag{19}$$

where

$$a = A_k^2(\beta) > 0, \qquad b = 2d_kA_k(\beta), \qquad r_0^2 = |\mathbf{d}|^2 \tag{20}$$

in which

$$A_k(\beta) = \left.\frac{\partial x_k}{\partial t_1}\right|_{\substack{t_1=c_1\\ t_2=c_2}} \left[(t_1^1 - t_1^0) + (t_1^2 - t_1^1)\beta\right] + \left.\frac{\partial x_k}{\partial t_2}\right|_{\substack{t_1=c_1\\ t_2=c_2}} \left[(t_2^1 - t_2^0) + (t_2^2 - t_2^1)\beta\right]. \tag{21}$$

The new distance function in (α, β) system is defined as

$$g(\alpha,\beta) = \sqrt{\left(\alpha + \frac{b}{2a}\right)^2 + \delta^2}. \tag{22}$$

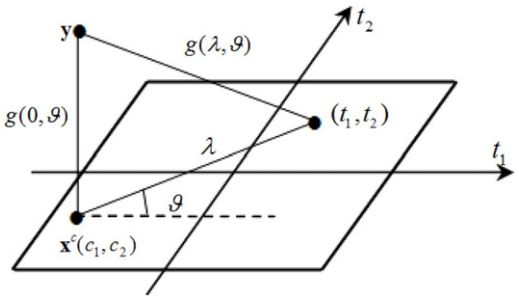

Fig. 6. The distance function $g(\lambda, \vartheta)$ depicted in the local (t_1, t_2) system.

It is noted that the system (α, β) is analogous to the system (ρ, θ), because the performances of α and β are very similar to ρ and θ, respectively. However, this new system is much more simple and even more effective than the polar system. This is partially due to the fact that both α and β are constrained to the interval [0, 1] in each triangle, and there is no need to calculate their spans. On the contrary, the spans for both ρ and θ in the polar system are needed to be determined complicatedly in each triangle for different types of boundary elements.

Until now, two distance functions are constructed in two local systems, which play an important role in the following distance transformation technique to remove or weaken near singularities arising in the integral of Eq. (6).

Considering the common features between two distance functions described by Eqs. (14) and (22), the following general distance function can be written as

$$g(\lambda, \vartheta) = \sqrt{\left(\lambda + \frac{b}{2a}\right)^2 + \delta^2} \tag{23}$$

where the pair(λ, ϑ)stands for (ρ, θ) and (α, β) in the polar system and the new (α, β) system, respectively. a and b are also obtained by Eqs. (13) and (20) for different local systems. The Jacobians for two transformations from the (t_1, t_2) system to different local systems are expressed in the following general form:

$$J(\lambda, \vartheta) = \kappa\lambda \tag{24}$$

where $\kappa = 1$ for the (ρ, θ) system, while $\kappa = S_\Delta$ for the (α, β) system.

As shown in Fig. 6, the distance function $g(\lambda, \vartheta)$ and $g(0, \vartheta)$ stand for the distance and the minimum distance, respectively. After applying special variable transformations, the function $g(\lambda, \vartheta)$ is just as a Jacobian. This is why the authors of Refs. [17,18] have dubbed the methodology *distance transformation*. In our implementation, distance transformations are discussed in the following section.

4. Distance transformation and in combination with element subdivision

4.1. Construct distance transformations

In this section, we construct distance transformations based on the distance functions detailed in the previous section to calculate nearly singular integrals over 3D boundary elements.

Now, we first introduce a pair of transformations for the integration variables in the local systems (ρ, θ) and (α, β), which are expressed as

$$\eta(\lambda, \vartheta) = \log\left(\lambda + \frac{b}{2a} + g(\lambda, \vartheta)\right) \tag{25a}$$

$$\lambda(\eta) = \frac{1}{2}[\exp(\eta) - \delta^2 \exp(-\eta)] - \frac{b}{2a}. \tag{25b}$$

This transformation is performed only in the radial variable λ, which is similar to various non-linear variable transformation methods. After performing the logarithmic transformation above, initial integrands are smoothed and the integration points are concentrated near the projection point, which can weaken the near singularities. What is more, the transformation Jacobian from λ to η is just as the distance function $g(\lambda, \vartheta)$, which serves as a weight that plays an important role of damping-out the near singularities of the integrands [17,18].

After splitting the integration element into several triangles based on the position of the projection and substituting Eq. (25a) into Eq. (6), the integrals on each triangle can be calculated using the standard Gaussian quadrature accurately

with the following form

$$I = \int_{\vartheta_1}^{\vartheta_2}\int_0^{\lambda_2} O(1/r^{\chi})\phi(\lambda,\vartheta)G(\lambda,\vartheta)J(\lambda,\vartheta)\mathrm{d}\lambda\mathrm{d}\vartheta$$
$$= \int_{\vartheta_1}^{\vartheta_2}\int_{\eta(0)}^{\eta(\lambda_2,\vartheta)} g(\eta,\vartheta)O(1/r^{\chi})\phi(\eta,\vartheta)G(\eta,\vartheta)\kappa\lambda(\eta)\mathrm{d}\eta\mathrm{d}\vartheta \tag{26}$$

where ϑ_1, ϑ_2 and λ_2 are integration variables limits, which are constant in (α,β) system ($\vartheta_1 = 0$, $\vartheta_2 = 1$ and $\lambda_2 = 1$).

From Eq. (26), since $g(\eta,\vartheta)$ is with the same order of r, we clearly find that the near weak singularity can be completely removed by the transformation (25a) when $\chi = 1$. Near strong singularity can also be removed with this transformation when $\chi = 2$, discussion given below.

Considering the following integral

$$I' = \int_{\vartheta_1}^{\vartheta_2}\int_{\eta(0)}^{\eta(\lambda_2,\vartheta)} \frac{1}{r^2} g(\eta,\vartheta)\kappa\lambda(\eta)\mathrm{d}\eta\mathrm{d}\vartheta. \tag{27}$$

Substituting Eq. (12) or (19) results in

$$I' \approx \int_{\vartheta_1}^{\vartheta_2}\int_{\eta(0)}^{\eta(\lambda_2,\vartheta)} \frac{1}{a}\frac{1}{g(\eta,\vartheta)^2} g(\eta,\vartheta)\kappa\lambda(\eta)\mathrm{d}\eta\mathrm{d}\vartheta$$
$$= \int_{\vartheta_1}^{\vartheta_2}\int_{\eta(0)}^{\eta(\lambda_2,\vartheta)} \frac{1}{a} f(\eta,\vartheta)\mathrm{d}\eta\mathrm{d}\vartheta \tag{28}$$

where

$$f(\eta,\vartheta) = \lambda(\eta)/\sqrt{\left(\lambda(\eta)+\frac{b}{2a}\right)^2+\delta^2}. \tag{29}$$

In most cases, b is zero in our implementation, which results in Eq. (29) being not a near singularity when δ^2 is small. If b is not zero, but with very small value when the nearly singular integrals arise, hardly introducing near singularity. The numerical tests in this paper have demonstrated the transformation (25a) is efficient to deal with nearly strong singular integrals.

When b is zero, the transformation given by Ref. [17] can also be employed to remove near strong singularity in integral (6). These transformation pairs are expressed as follows:

$$\eta(\lambda,\vartheta) = \log(g(\lambda,\vartheta)) \tag{30a}$$
$$\lambda(\eta) = \sqrt{\exp(2\eta)-\delta^2}. \tag{30b}$$

In a similar manner, the integrals for each triangle can be calculated numerically with the following expression:

$$I = \int_{\vartheta_1}^{\vartheta_2}\int_0^{\lambda_2} O(1/r^{\chi})\phi(\lambda,\vartheta)G(\lambda,\vartheta)J(\lambda,\vartheta)\mathrm{d}\lambda\mathrm{d}\vartheta$$
$$= \int_{\vartheta_1}^{\vartheta_2}\int_{\eta(0)}^{\eta(\lambda_2,\vartheta)} g^2(\eta,\vartheta)O(1/r^{\chi})\phi(\eta,\vartheta)G(\eta,\vartheta)\kappa\mathrm{d}\eta\mathrm{d}\vartheta. \tag{31}$$

The transformation (30a) can completely remove near strong singularity when $\chi = 2$, and is also effective to remove near weak singularity when $\chi = 1$.

4.2. Distance transformation in combination with element subdivision

In this section, we subdivide an integration element in a suitable pattern considering both element shape and the position of the projection point $\mathbf{x}^c$ in the element, and adaptive integration technique based on element subdivision is employed in combination with our distance transformation. The adaptive integration technique is discussed in detail in Ref. [1,20].

Note that although the original quadrangle has a good shape, the four subtriangles may have unsuitable shapes depending on the position of $\mathbf{x}^c$ (see Fig. 7(a)). Obtaining good shaped triangles seems more difficult with direct subdivision for irregular initial elements as shown in Fig. 7(b) and (c) even $\mathbf{x}^c$ located at the element's center. If the angle denoted as θ in Fig. 7(a) between two lines in common with end point $\mathbf{x}^c$ in each triangle is larger than a certain value and even tends to π, numerical results will become less accurate. This has been demonstrated by subsequent numerical tests in this paper.

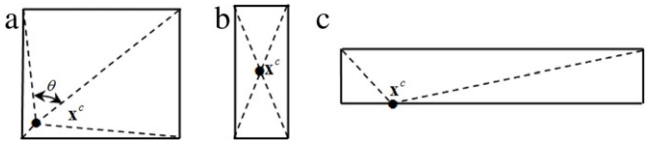

Fig. 7. Subdivisions of quadrilateral elements with triangles.

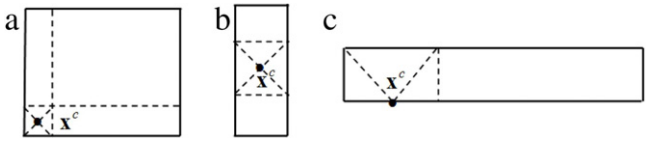

Fig. 8. Adaptive subdivisions of quadrilateral elements.

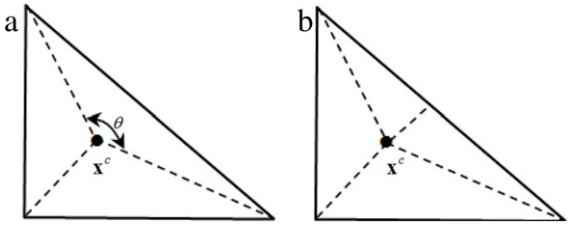

Fig. 9. Two types of subdivisions for a triangular element: (a) ordinary subdivisions; (b) improved subdivisions.

To avoid the unsuitable cases described above, we have developed an adaptive subdivision for an arbitrary quadrilateral element. The original element is divided into several triangles and additional quadrangles, which is different from that as shown in Fig. 7. The adaptive subdivision consists of mainly three steps described briefly as follows:

- First, compute the distances in the real-word-coordinate system form $\mathbf{x}^c$ to each edge of the element and obtain the minimum distance l.
- Then, based on l, we construct a box defined in a parametric system, but with possibly the square shape in the real-word-coordinate system, well-covering $\mathbf{x}^c$.
- Finally, triangles are constructed in the box and additional quadrangles are created in element's remaining region outside the box.

Applying the strategy above, adaptive subdivisions for the elements in Fig. 7 with suitable patterns are shown in Fig. 8. For each triangle, the nearly singular integrals are calculated by the scheme discussed in Section 4. However, for each quadrangle, nearly singular integrals will arise but not severely, which can be calculated by an adaptive integration scheme based on the element subdivision technique discussed in Ref. [1,20]. The subdivision is performed using an adaptive tree structure.

It should be noted that, although the element subdivision is adopted, the cost can be reduced dramatically compared with the conventional subdivision techniques [1,6,20]. This is because, in the combined method, the integral over regions of the element that are very near to the source point is calculated by the distance transformation technique, while the integral over the remained region is calculated by element subdivision technique. Therefore, the overall integration points are significantly reduced.

Now, we discuss how to divide a triangular element in a suitable pattern. As shown in Fig. 9(a), subdividing an integration triangle into several subtriangles in an ordinary way, will result in the angular θ tending to π in a subtriangle. The subdivisions are not suitable for obtaining accurate numerical integrals. In this case, if θ of a subtriangle described in Fig. 9(a) is more than a certain value φ, we subdivide the subtriangle into two triangles through the bisector of θ. According to the numerical tests, we have set $\varphi = 2\pi/3$. This strategy is analogous to the related method suggested in [5]. The improved subdivisions are shown in Fig. 9(b) by applying our strategy.

5. Numerical examples and discussions

To validate the accuracy as well as the efficiency of the current method, this section presents several numerical examples for the evaluation of nearly singular integrals over different elements. To conveniently describe the influence of the nearly singular integrals over each element, the relative distance is given in the terms of $r_0/a^{1/2}$, where a stands for element's area, and r_0 is the minimum distance (see Eq. (13) or (20)). For the purpose of error estimation, the relative error is defined as follows:

$$error = \frac{I_{nume} - I_{exact}}{I_{exact}} \tag{32}$$

Table 1
Relative errors of the integrals with kernels u^* and $1/r^2$ on a triangular element when the projection point is located inside it.

$r_0/a^{1/2}$	10^{-1}	10^{-2}	10^{-3}	10^{-4}	10^{-5}	10^{-6}
Reference solution	0.154994	0.183112	0.186256	0.186574	0.186606	0.186609
u^*	8.39E−9	2.12E−8	2.29E−8	2.31E−8	2.30E−8	2.20E−8
Reference solution	10.201568	24.514607	38.980575	53.448128	67.915696	82.383265
$1/r^2$	3.06E−8	1.26E−7	−4.46E−7	−3.53E−6	5.05E−6	3.26E−5

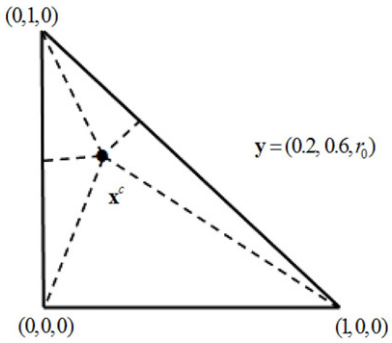

Fig. 10. A triangular element and its subdivisions when the projection point is located inside it.

Table 2
Relative errors of various integrals with kernel u^* on a triangle element when the projection point is located on an edge of it.

$r_0/a^{1/2}$	10^{-1}	10^{-2}	10^{-3}	10^{-4}	10^{-5}	10^{-6}
Exact solution	0.108780	0.134583	0.139447	0.140166	0.140261	0.140273
u^*	1.38E−10	−4.10E−9	−6.20E−9	−6.61E−9	−6.71E−9	−7.67E−9

where the subscripts *nume* and *exact* refer to the numerical and exact solutions, respectively. Note that if the exact solution is not available, a reference solution obtained by semi-analytical methods or subdivision technique with enough subelements, is regarded as the exact solution. We use 10×10 point Gaussian quadratures over each subtriangle in all cases for the convenience of comparison and assume $\phi(\eta, \vartheta) = 1$ in Eqs. (26) and (31) if it is not specified.

In the following text, numerical examples will be investigated based on the different 3D surface elements including planar triangular elements, planar quadrilateral elements with irregular and regular shape, and a curved quadrilateral element.

5.1. Triangular element

The first example considers nearly singular integrals on a planar triangular boundary element with the node coordinates of (0,0,0), (1,0,0) and (0,1,0). Two cases are discussed here regarding position of the projection point of the given source point, namely, being inside and on an edge of the element.

For the first case, the source point coordinates are set to $(0.2, 0.4, r_0)$ as shown in Fig. 10. This problem is taken from Ref. [5]. As the exact solution is not available, a reference solution is obtained by the sim-analytical method described in Ref. [5]. Based on the strategy of subdivision suggested in Section 4, the element is split into five triangular patches before applying the distance transformation technique (seen Fig. 10). For each patch, formulation (26) with new transformation (25a) based on the local (α, β) system, is used to compute nearly singular integrals with the kernels u^* and $1/r^2$, respectively. Table 1 presents the relative errors of various integrals for different values of $r_0/a^{1/2}$. It is found that the order of the relative accuracy is less than 10^{-7} for kernel u^*, even when the relative distance reaches up to 10^{-6}. And the results for kernel $1/r^2$ are also accurate. These attractive results have demonstrated our method is very efficient.

For the second case, the source point coordinates are set to $(d, d, 0)$ as shown in Fig. 11. d is obtained by the following expression:

$$d = \frac{\sqrt{2}}{2} + r_0 \sin\left(\frac{\pi}{4}\right). \tag{33}$$

For this special problem, after subdividing the element into two triangular patches by the broken line with an end point $\mathbf{x}^c$ (see Fig. 11), the exact solution of the integrals for the kernel u^* can be obtained easily in an analytical way. The local (α, β) system is also employed. Given a set of values of $r_0/a^{1/2}$, the results obtained by Eq. (26) are presented in Table 2. Again, from the table, highly accurate results are achieved compared with exact solutions.

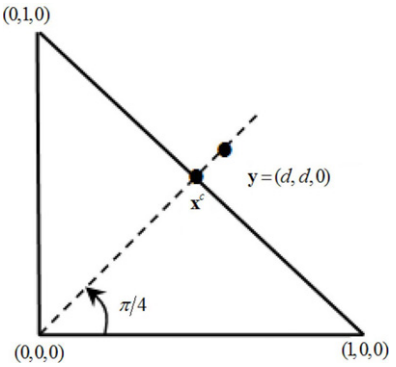

Fig. 11. A triangular element and its subdivisions when the projection point is located on an edge of it.

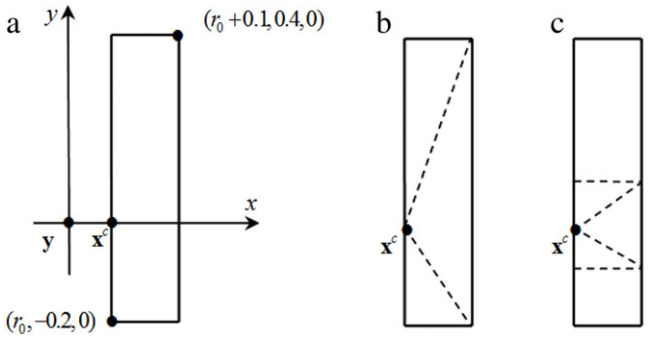

Fig. 12. Nearly singular integration on an irregular quadrilateral element: (a) the element's geometric size; (b) conventional subdivision; (c) improved subdivision.

Remark 1. The local (α, β) system is first introduced here for accurate computation of nearly singular integrals over triangular elements. The system is simpler than the local polar (ρ, θ) system, in which the upper and lower limits of both ρ and θ are need to be given with different values in different triangular patches. And the numerical tests above have shown that (α, β) system is very efficient in evaluation of the nearly singular integrals.

Remark 2. Considering the second case above, point $\mathbf{x}^c$ will be located outside the element based on the definition of the projection point in Ref. [17,18], which make it difficult to determine the limits of integration variables in (ρ, θ) system even in the new (α, β) system. However, this problem has been avoided by applying our method based on the improved definition of the projection point, which is always located inside the element or on an edge or a vertex of the element.

5.2. Irregular quadrilateral element

Computing nearly singular integrals over an irregular quadrilateral element is considered as the second example, to verify distance transformation in combination with adaptive integration based on element subdivision. This type of element is employed usually instead of using many smaller elements when slender or thin structures are concerned or in cases where the boundary element distribution on a surface is very irregular. The element's geometric size is given in Fig. 12(a).

In order to assess the combined method, numerical results are obtained in two different patterns of the element subdivision, as shown in Fig. 12(b) and (c). Fig. 12(b) depicts the conventional subdivision, while Fig. 12(c) shows an improved subdivision to be used in the combined method. Two local systems (α, β) and (ρ, θ) are used in each case. The results obtained by Eq. (26) are presented in Tables 3 and 4 for various integrals with the kernels u^* and u^*_x, respectively. The exact solutions of integrals with kernel u^* can be available with the related method in Ref. [6].

In the two tables, symbol *NDivd* denotes the results are obtained by the distance transformation technique only, while symbol *Divd* denotes the results are obtained by the distance transformation technique in combination with adaptive integration. The tabulated results clearly show that, for the same relative distance, the results obtained with the combined method are more accurate than that of only distance transformation technique. With the combined method, we have a relative accuracy less than10^{-5} for the kernel u^*, even the relative distance at 10^{-6}. And we have a relative accuracy less than 10^{-4} for the kernel u^*_x in all cases. From the two tables, it is also found that the results obtained in (α, β) system are better than that in (ρ, θ) system for the most cases when the combined method is adopted.

Table 3
Relative errors of various integrals with kernel u^* in an irregular quadrilateral element.

$r_0/a^{1/2}$		10^{-1}	10^{-2}	10^{-3}	10^{-4}	10^{-5}	10^{-6}
Exact solution		0.0340406	0.0418669	0.0434211	0.0436569	0.0436886	0.0436926
(ρ, θ)	*NDivd*	−4.49E−6	−6.20E−5	−9.66E−5	−1.04E−4	−1.05E−4	−1.05E−4
	Divd	−1.98E−6	−1.60E−6	−1.52E−6	−1.51E−6	−1.51E−6	−1.51E−6
(α, β)	*NDivd*	−1.69E−5	−1.46E−4	−2.12E−4	−2.26E−4	−2.28E−4	−2.28E−4
	Divd	−1.00E−10	−9.00E−10	−1.90E−9	−2.10E−9	−2.20E−9	−2.50E−9

Table 4
Relative errors of various integrals with kernel u_x^* in an irregular quadrilateral element.

$r_0/a^{1/2}$		10^{-1}	10^{-2}	10^{-3}	10^{-4}	10^{-5}	10^{-6}
Reference solution		0.2504831	0.5881625	0.9514044	1.3175456	1.6839807	2.0504452
(ρ, θ)	*NDivd*	−6.81E−5	−7.93E−4	−1.37E−3	−1.66E−3	−1.81E−3	−1.91E−3
	Divd	−2.17E−7	4.23E−7	−2.06E−7	1.32E−6	1.73E−5	3.28E−5
(α, β)	*NDivd*	−2.08E−4	−1.60E−3	−2.56E−3	−3.05E−3	−3.31E−3	−3.35E−3
	Divd	−7.00E−10	9.80E−9	−8.42E−7	5.78E−7	1.65E−5	3.20E−5

Table 5
Relative errors of various integrals with kernel u^* on a cylindrical surface element.

$r_0/a^{1/2}$	10^{-1}	10^{-2}	10^{-3}	10^{-4}	10^{-5}	10^{-6}
Reference solution	0.0077988	0.0079031	0.0079136	0.0079147	0.0079148	0.0079148
(ρ, θ)	−6.42E−9	−2.52E−7	−1.99E−6	−6.09E−6	−7.44 E−6	9.11 E−6
(α, β)	−7.16E−9	−2.52E−7	−1.99E−6	−6.09E−6	−7.44 E−6	9.11 E−6

Table 6
Relative errors of various integrals with kernel q^* on a cylindrical surface element.

$r_0/a^{1/2}$	10^{-1}	10^{-2}	10^{-3}	10^{-4}	10^{-5}	10^{-6}
Reference solution	0.2839962	0.2890126	0.2895177	0.2895683	0.2895733	0.2895738
(ρ, θ)	1.81E−7	−4.48E−6	1.59E−6	7.89E−5	1.77E−4	1.50E−4
(α, β)	1.76E−7	−4.48E−6	1.58E−6	7.89E−5	1.77E−4	1.50E−4

Remark 3. The distance transformation technique in combination with adaptive integration is a very efficient scheme to calculate nearly singular integrals over an irregular quadrilateral element. Actually, the strategy is also capable of dealing with the case when a quadrilateral element is regular, but the position of the projection point is close to an element's edge or vertex. Although adaptive integration scheme based on element subdivision is employed here, the cost of the element subdivision is reduced dramatically. It is because that the integrals on the element local region that is very near to the source point are computed by the distance transformation technique, avoiding a large number of integration points concentrated near the projection point.

5.3. Curved surface element

The third example considers nearly singular integrals on a curved surface element. The curved surface element is represented in parametric form with the usual spherical polar system (θ, φ), and this kind of element is named as spherical surface element which is used in BFM usually [1,20]. The element's geometric parameters are given as follows: $\theta \in [0, \pi/4]$, $\varphi \in [\pi/4, \pi/2]$, the sphere radius $r = 0.1$, and with center (0, 0, 0). The projection point of the fixed source point is located at the element's center. To obtain shape function values in general form, we regularize θ and φ within the interval $[-1, 1]$, and then the corresponding spherical system is described by the system $[t_1, t_2]$. As this surface element is distorted from (θ, φ) to $[t_1, t_2]$, the transformation Jacobian is not constant. Unlike previous examples with constant shape function $\phi = 1$, a higher order shape function is involved in this special example. The shape function is expressed as:

$$\phi\left((t_1(\eta, \vartheta), t_2(\eta, \vartheta))\right) = \left(1 - t_1^2(\eta, \vartheta)\right)\left(1 + t_2(\eta, \vartheta)\right)/2. \tag{34}$$

Various integrals are computed by Eq. (26) in two local systems. The relative errors are listed in Tables 5 and 6 for the kernels u^* and q^*, respectively. It is found that the relative errors are very small with the order less than 10^{-5} for integrals with kernel u^*, namely the numerical results are very accurate. It is also found that, for integrals with kernel q^*, relative errors increase up to 10^{-4}. Although the results are not good as those in the planar elements, the accuracy is enough for the most actual engineering applications up to the range of $r_0/a^{1/2} = 10^{-4}$ and the results are still acceptable even $r_0/a^{1/2}$ up to 10^{-6}.

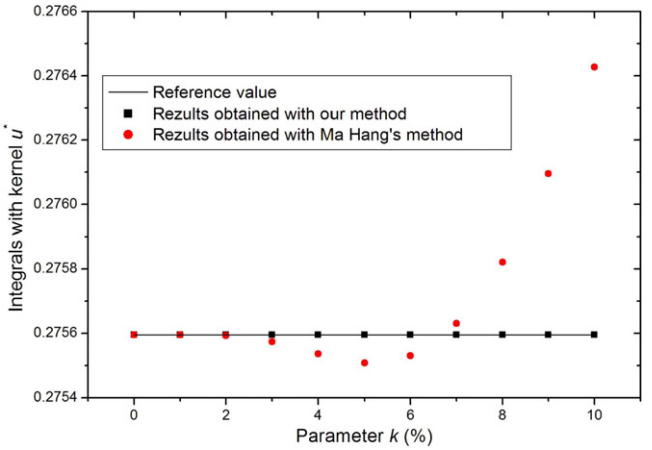

Fig. 13. Various integrals with kernel u^* against the offset parameter.

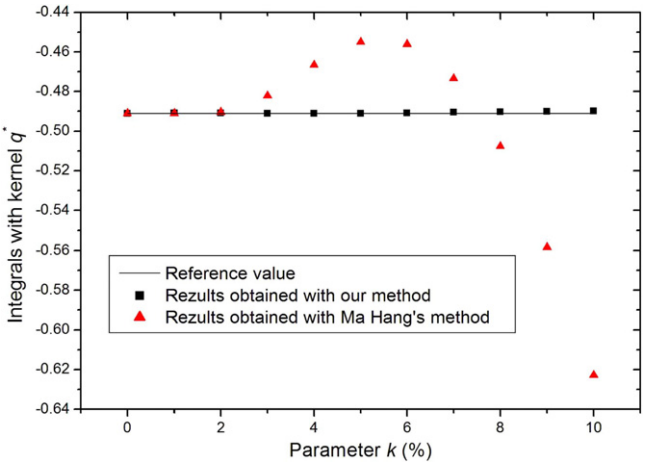

Fig. 14. Various integrals with kernel q^* against the offset parameter.

Remark 4. The present method is capable of computing nearly singular integrals on both planer and curved elements, which can be directly used for the isoparametric elements with high order shape functions in BEM.

5.4. Regular quadrilateral element

In this section, we study the influence of the position of the projection point on the accuracy of our method when the source point is fixed. In this study, we compute nearly singular integrals in different cases on a regular quadrilateral element with the node coordinates (0, 0, 0), (1.0, 0, 0), (1.0, 1.0, 0) and (0, 1.0, 0). For each case, the source point is fixed at (0.5, 0.5, 0.01), and the projection point $\mathbf{p}$ is determined by an offset parameter k, $0 \leq k \leq 1$, using the following equation:

$$\mathbf{p} = \mathbf{x}^c + k\mathbf{x}^c \tag{35}$$

where $\mathbf{x}^c$ is the ideal projection point at the center of the element with coordinates (0, 0) in local (t_1, t_2) system if we constrain both t_1 and t_2 to the span $[-1, 1]$. Obviously, the projection point $\mathbf{p}$ is coincident with the ideal projection point $\mathbf{x}^c$ when $k = 0$.

Given a set of values of k, all computations have been performed with our method using Eq. (26) and the method suggested in [17,18] using Eq. (31), respectively. Numerical results and the reference values of various integrals are shown in Figs. 13 and 14 for the kernels u^* and q^*, respectively. It is obviously seen that the results obtained with our method are in good agreement with the reference values even when the offset parameter k increases up to 10%, namely, the accuracy of our method is not sensitive to the position of the projection point. On the contrary, the results obtained with Ma Hang's method are very sensitive to the position of projection, and when the parameter k increases to a certain value, the results become very poor.

Remark 5. As we know, finding the ideal projection point is an very important step for successful implementation of the most of methods to deal with nearly singular integrals. This is why the results from those methods are largely dependent on the position of the projection point. Since the results of our method are not sensitive to the projection point's position, our method becomes very competitive when it is inconvenient to locate the ideal projection point. Actually, the ideal projection point is not always available in many actual problems.

6. Conclusions

A general method, which is based on an improved distance transformation, is presented to efficiently compute nearly singular integrals arising in the BIEs on different types of 3D boundary elements. In our method, the improved distance transformations are derived from two novel distance functions based on the two local systems described by (ρ, θ) and (α, β), respectively. (α, β) system is first employed to deal with nearly singular integrals, which is simpler than (ρ, θ) system and is also efficient. In each local system, the distance function is constructed by applying the first-order Taylor expansion in the neighborhood of the projection point. We have proposed a more general definition of the projection point. This is an important feature of the present method, because the drawbacks of the conventional distance transformation technique can be avoided. We have also developed an adaptive element subdivision considering both element shape and the position of the projection point, and have successfully integrated the improved distance transformation technique with an adaptive integration technique.

The present method has been verified through a number of numerical examples with different boundary elements, kernel functions and relative distances. It was observed that our method can compute integrals with near weak and strong singularities accurately and efficiently, even when the relative distance reaches up to 10^{-6}. What's more, the accuracy of our method is much less sensitive to the position of the projection point than conventional distance transformation. Actually, combining with the Stoke's theorem as Ref. [17], our method can be easily extended to deal with nearly hypersingular integrals.

Acknowledgements

This work was supported in part by National 973 Project of China under grant number 2010CB328005, and in part by National Science Foundation of China under grant number 10972074.

References

[1] J.M. Zhang, X.Y. Qin, X. Han, G.Y. Li, A boundary face method for potential problems in three dimensions, Internat. J. Numer. Methods Engrg. 80 (2009) 320–337.
[2] Y.J. Liu, Analysis of shell-like structures by the boundary element method based on 3-D elasticity: formulation and verification, Internat. J. Numer. Methods Engrg. 41 (1998) 541–558.
[3] Y.J. Liu, H. Fan, Analysis of the thin piezoelectric solids by the boundary element method, Comput. Methods Appl. Mech. Engrg. 191 (2002) 2297–2315.
[4] X.W. Gao, T.G. Davies, Adaptive integration in elasto-plastic boundary element analysis, J. Chin. Inst. Eng 23 (2000) 349–356.
[5] Scuderi Letizia, On the computation of nearly singular integrals in 3D BEM collocation, Internat. J. Numer. Methods Engrg. 74 (2007) 1733–1770.
[6] L. Jun, G. Beer, J.L. Meek, Efficient evaluation of integrals of order $1/r$, $1/r^2$, $1/r^3$ using Gauss quadrature, Eng. Anal. 2 (1985) 118–123.
[7] Z.R. Niu, W.L. Wendland, X.X. Wang, H.L. Zhou, A sim-analytic algorithm for the evaluation of the nearly singular integrals in three-dimensional boundary element methods, Comput. Methods Appl. Mech. Engrg. 31 (2005) 949–964.
[8] H.L. Zhou, Z.R. Niu, C.Z. Cheng, Z.W. Guan, Analytical integral algorithm applied to boundary layer effect and thin body effect in BEM for anisotropic potential problems, Comput. Struct. 86 (2008) 1656–1671.
[9] J.C.F. Telles, A self-adaptive co-ordinates transformation for efficient numerical evaluation of general boundary element integrals, Internat. J. Numer. Methods Engrg. 24 (1987) 959–973.
[10] X.L. Chen, Y.J. Liu, An advanced 3-D boundary element method for characterizations of composite materials, Eng. Anal. Bound. Elem. 29 (2005) 513–523.
[11] K. Hayami, Variable transformations for nearly singular integrals in the boundary element method, Publ. Res. Inst. Math. Sci. 41 (2005) 821–842.
[12] B.M. Johnston, P.R. Johnston, D. Elliott, A sinh transformation for evaluating two-dimensional nearly singular boundary element integrals, Internat. J. Numer. Methods Engrg. 69 (2007) 1460–1479.
[13] P.R. Johnston, Application of sigmoidal transformation to weakly singular and nearly-singular boundary element integrals, Internat. J. Numer. Methods Engrg. 45 (1999) 1333–1348.
[14] Y.M. Zhang, Y. Gu, J.T. Chen, Boundary layer effect in BEM with high order geometry elements using transformation, (CMES) Comput. Mod. Eng. Sci. 45 (2009) 227–247.
[15] Y.M. Zhang, Y. Gu, J.T. Chen, Boundary element analysis of the thermal behaviour in thin- coated cutting tools, Eng. Anal. Bound. Elem. 34 (2010) 775–784.
[16] S. Wu, On the evaluation of nearly singular kernel integrals in boundary element analysis, Numer. method Eng. 11 (1995) 331–337.
[17] H. Ma, N. Kamiya, Distance transformation for the numerical evaluation of near singular boundary integrals with various kernels in boundary element method, Eng. Anal. Bound. Elem. 26 (2002) 329–339.
[18] H. Ma, N. Kamiya, A general algorithm for the numerical evaluation of nearly singular boundary integrals of various orders for two- and three-dimensional elasticity, Comput. Mech. 29 (2002) 277–288.
[19] M. Guiggiani, N. Gigante, A general algorithm for multi-dimensional Cauchy principal value integrals in the boundary element method, (ASME) J. Appl. Mech. 57 (1990) 906–915.
[20] X.Y. Qin, J.M. Zhang, G.Y. Li, et al., An element implementation of the boundary face method for 3D potential problems, Eng. Anal. Bound. Elem. 34 (2010) 934–943.